ENVIRONMENTAL SCIENCE

Global soil pollution by toxic metals threatens agriculture and human health

Deyi Hou[1,2]*†, Xiyue Jia[1]†, Liuwei Wang[1], Steve P. McGrath[3], Yong-Guan Zhu[4,5], Qing Hu[6], Fang-Jie Zhao[7], Michael S. Bank[8,9], David O'Connor[10], Jerome Nriagu[11]

Toxic metal pollution is ubiquitous in soils, yet its worldwide distribution is unknown. We analyzed a global database of soil pollution by arsenic, cadmium, cobalt, chromium, copper, nickel, and lead at 796,084 sampling points from 1493 regional studies and used machine learning techniques to map areas with exceedance of agricultural and human health thresholds. We reveal a previously unrecognized high-risk, metal-enriched zone in low-latitude Eurasia, which is attributed to influential climatic, topographic, and anthropogenic conditions. This feature can be regarded as a signpost for the Anthropocene era. We show that 14 to 17% of cropland is affected by toxic metal pollution globally and estimate that between 0.9 and 1.4 billion people live in regions of heightened public health and ecological risks.

Soil provides the basis for nearly 95% of food consumed by human beings (*1*). As the human population continues to grow and living standards improve, global food production needs to increase by 35 to 56% by 2050 (*2*). This puts substantial pressure on nonrenewable soil resources, the degradation of which already threatens the livelihoods of 1.3 billion people globally (*3*). The United Nations Food and Agriculture Organization (FAO) warns that 90% of global soil resources may be at risk by 2050, owing to soil erosion, excessive usage of fertilizers and pesticides, and industrial pollution (*4*, *5*). Often overlooked in the matter of soil quality is soil pollution by toxic heavy metals and metalloids (herein "toxic metals"), which reduces crop yields and results in unsafe food. Even though some metals such as cobalt (Co) and copper (Cu) are essential in small amounts for biological functioning, their bioaccumulation in organisms, including crops, can render them toxic in the human food chain. Furthermore, toxic metals are nondegradable and therefore accumulate over decadal timescales in soils (*6*–*8*).

Global soil pollution by toxic metals has been studied for decades (*9*); however, quantitative estimates of their impact on soil quality and spatially explicit mapping of soil pollution on a global scale are lacking. A few regional and country-scale investigations have provided concerning data on this issue. For instance, a national survey in China found that 19% of agricultural soils exceeded soil quality standards, with arsenic (As, a metalloid), cadmium (Cd), Cu, and nickel (Ni) accounting for the majority of exceedances (*10*). A study on toxic metals across 27 European countries showed that 28% of soils exceeded thresholds (*11*).

There are two main sources of toxic metals in soil: geogenic and anthropogenic. Toxic metals are ubiquitous in bedrocks, which are the natural soil parent materials, and occur in varying concentrations. Some types of parent rock (e.g., basalt and shale), as well as primary minerals (e.g., pyrite, sphalerite), contain elevated levels of As, Cd, Cu, and Ni that result from the high affinity of sulfur for these metals (*8*, *12*). During the geologic weathering and soil-forming processes, toxic metals are continuously released from soil parent materials (*13*, *14*). Some toxic metals may also be transported in the atmosphere after volcanic emissions and wind erosion and subsequently deposited in surface soil (*13*, *15*). Because of translocation and transformation mechanisms occurring during pedogenesis, toxic metals may accumulate in soil because of fixation in crystal lattices—binding with clay minerals through electrostatic forces—or complexation with organic matter and iron (Fe) oxyhydroxides, which can lead to a high natural background of toxic metal concentrations in certain soil environments (*12*, *16*, *17*).

Anthropogenic sources of toxic metals in the pedosphere include agricultural, household, and industrial activities. Substantial metal contamination of soils commenced at the beginning of the Anthropocene (e.g., Bronze Age), particularly as a result of metal mining and processing (*13*, *18*). Mining activities transfer huge quantities of rock, often with high metal concentrations, from the underground to the surface. This leads to soil pollution by leachate and runoff from mining waste, irrigation of cropland with polluted water, wind-eroded waste rocks, and atmospheric deposition originating from metal smelters (*6*, *19*). Metal pollution at a given location may be transported across long distances, as evidenced by ice cores recovered from Greenland, which reveal that intensive mining and smelting activities in the Greek and Roman times caused pronounced pulse in metal contamination at hemispheric scales (*20*). Elevated toxic metal contents are also embedded in industrial infrastructure (including machinery, bridges, transport systems, cables, and buildings) and agricultural and household products (such as phosphorus fertilizers, paints, and batteries), which can contribute considerably to the toxic metal burden in soil ecosystems (*21*).

The spatial distribution of toxic metals in soil depends on a dynamic and complex balance between input and output processes. The main output pathways include leaching, soil erosion by surface runoff, plant uptake, and crop harvest (*13*, *17*, *22*). Redistribution of toxic metals may occur in the vertical dimension of soil profiles because of soil-plant interactions. The plant-pump effect, for instance, transports toxic metals from deeper soil (e.g., C horizons) to surficial soil (e.g., O horizons), where they accumulate (*17*). Toxic metals in soil may also migrate at regional scales because of biovolatization, wind-borne soil suspension, forest fires, and other perturbances (*13*, *15*). On the basis of these migration mechanisms, it has been suggested that certain environmental and socioeconomic factors, including topography, climate, soil texture, and human activities, may be used as predictors to evaluate toxic metal distribution across large spatial scales (*11*, *23*–*25*).

The combination of recent developments in machine learning technologies and the availability of expansive measurement data now make it possible to undertake a systematic assessment of global soil pollution for seven toxic metals: As, Cd, Co, chromium (Cr), Cu, Ni, and lead (Pb). We hypothesized that soil pollution, on a global scale, would be governed by both direct and indirect effects of biogeophysical and anthropogenic factors. Using machine learning models, we identified and analyzed multilayered and nonlinear relationships and developed a robust and spatially explicit, continuous prediction of toxic metal exceedances on the basis of sparsely distributed global data.

Global toxic metal exceedances

We have compiled 796,084 datapoints of soil concentrations of the key toxic metals from 1493 regional studies covering diverse climate zones, geologic settings, and land use types (figs. S1 and S2) (*26*). Data quality assurance procedures were followed to ensure that the

[1]School of Environment, Tsinghua University, Beijing, China. [2]State Key Laboratory of Regional Environment and Sustainability, Tsinghua University, Beijing, China. [3]Rothamsted Research, Sustainable Soils and Crops, Harpenden, United Kingdom. [4]Research Center for Eco-Environmental Sciences, Chinese Academy of Sciences, Beijing, China. [5]Institute of Urban Environment, Chinese Academy of Sciences, Xiamen, China. [6]Engineering Innovation Centre (Beijing), Southern University of Science and Technology, Shenzhen, China. [7]College of Resources and Environmental Sciences, Nanjing Agricultural University, Nanjing, China. [8]Institute of Marine Research, Bergen, Norway. [9]Department of Environmental Conservation, University of Massachusetts Amherst, Amherst, MA, USA. [10]School of Real Estate and Land Management, Royal Agricultural University, Cirencester, UK. [11]School of Public Health, University of Michigan, Ann Arbor, MI, USA.
***Corresponding author. Email: houdeyi@tsinghua.edu.cn**
†These authors contributed equally to this work.

data were reliable and representative of regional metal concentrations, and appropriate analytical methods were used to ensure robust measurements (*26*). Samples collected from studies focusing on contaminated sites were excluded to avoid bias toward highly enriched localized areas. Soil concentrations in 10 km by 10 km pixels were converted to binary data by using a set of agricultural thresholds (AT) and human health and ecological thresholds (HHET) derived from country thresholds (table S1) (*26*). Five sets of predictive variables, namely climatic, geological, soil textural, topographic, and socioeconomic, were included as proxies of natural and anthropogenic processes governing metal abundance in soil. Extremely randomized trees (ERT) was selected as the best-performing machine learning model (*27*). The models were validated with an independent dataset, which verified high model precision and accuracy unrelated to numerical overfitting. The models were then used to project data onto a soil pollution map on a global scale, excluding any permafrost and desert areas (*26*).

Globally, our model estimates that 14 to 17% (95% confidence interval) of surface soils exceed the AT for at least one toxic metal in cropland areas (Fig. 1). Probabilities of individual metal exceedance vary geographically (figs. S4 to S10). The global exceedance rate of Cd is the highest, reaching 9.0% (−1.9%/+1.5%). Cadmium exceedance for agricultural soil is the most notable in northern and central India, Pakistan, Bangladesh, southern China, southern parts of Thailand and Cambodia, Iran, Türkiye, Ethiopia, Nigeria, South Africa, Mexico, and Cuba. Both anthropogenic sources and geogenic enrichment likely contributed to the elevated Cd concentrations in these regions (*6*, *8*, *28*, *29*). The exceedance rates of Ni and Cr reach 5.8% (−1.8%/+1.1%) and 3.2% (−0.7%/+1.6%), respectively. Their exceedance is the most prevalent in the Middle East, subarctic Russia, and eastern Africa, likely due to high geogenic background as well as mining activities (*28*, *30*). Soil As exceedance occurred at a rate of 1.1% (−0.04%/+0.3%) and was the most notable in southern and southwestern China, south and Southeast Asia, West Africa, and central parts of South America, which coincides with observed and predicted areas of high As concentration in groundwater (*14*). The exceedance rate of Co is 1.1% (−0.1%/+2.9%) and was the most prevalent in Zambia, the Democratic Republic of the Congo, and Ethiopia, likely the result of mining-related activities

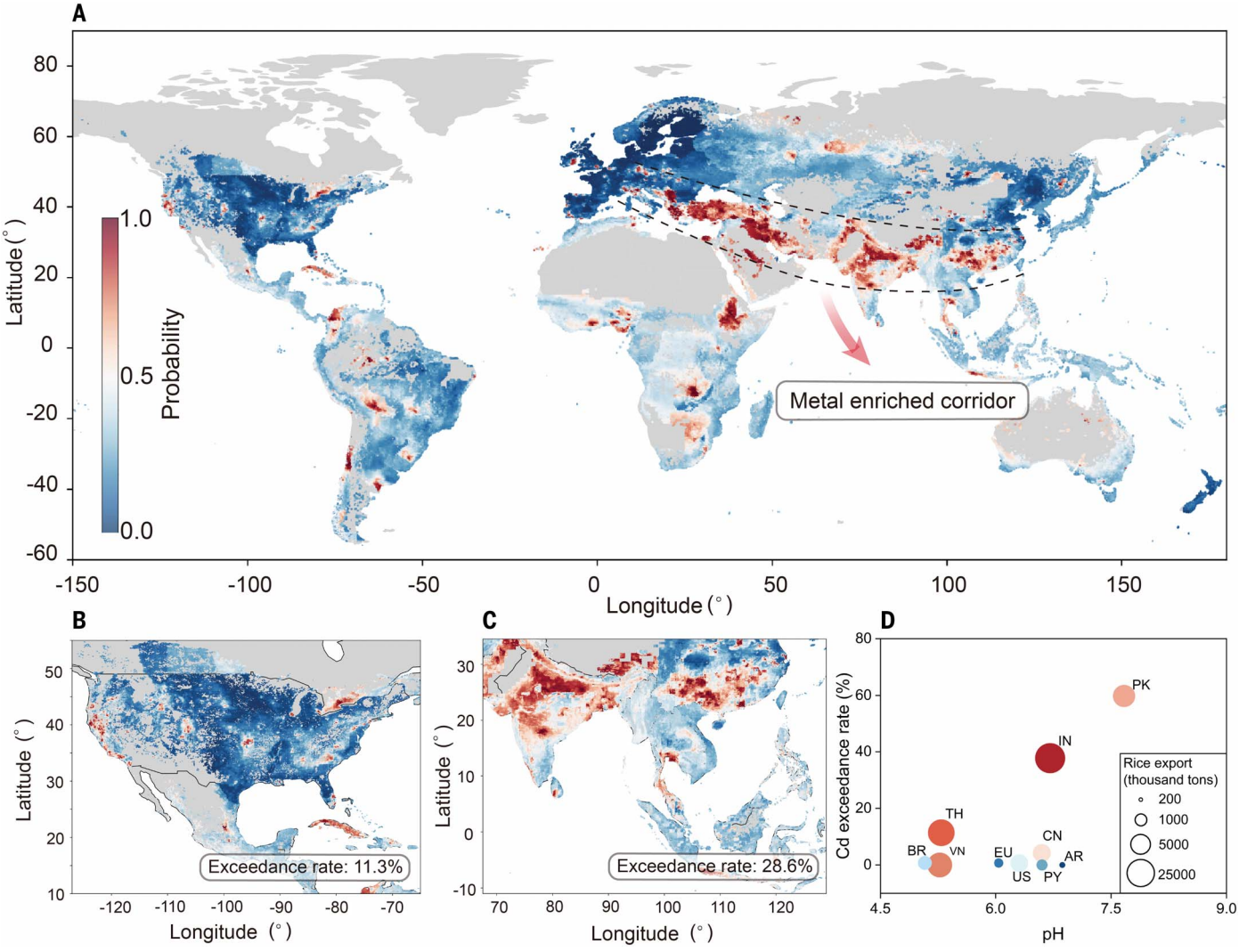

Fig. 1. Global soil pollution by toxic metals exceeding agricultural thresholds (AT). (**A**) Aggregate distribution of exceedance of arsenic, cadmium, cobalt, chromium, copper, nickel, and lead; color code shows the maximum probability of exceedance among the seven metals. (**B** and **C**) Zoomed-in sections of globally important food production areas. (**D**) Predicted Cd exceedance rates and average soil pH indicative of Cd mobility in the major rice export countries. Country abbreviation: IN, India; TH, Thailand; VN, Vietnam; PK, Pakistan; CN, China; US, United States; BR, Brazil; PY, Paraguay; EU, European Union; AR, Argentina.

(*31*). Globally, 6.8% (−1.7%/+1.9%) of surficial soil exceeded HHET, with a similar or smaller exceedance than AT exceedance owing to generally less stringent threshold values (Fig. 2 and figs. S11 to S17).

Soil pollution by toxic metals has considerable impacts on food production and food safety. We estimate that 242 million ha (−26/+27 million ha), or 16% of global cropland, is affected by toxic metal exceedances. Among the areas most at risk, southern China, northern and central India, and the Middle East are well documented to have elevated toxic metal concentrations in their soils (*32*–*34*). Limited data exist for Africa, and the prediction will require more soil sampling and analysis for verification (*35*).

By overlaying the human health and ecological risk map over global population distribution in 2020, it is estimated that 0.9 to 1.4 billion people live in the high-risk areas (Fig. 2B). However, it should be noted that the actual risks posed by soil metals are dependent upon their mobility, overall bioavailability, and human exposure pathway dynamics (*36*, *37*). Exposure and toxic effects also depend on individual dietary habits and food deprivation, as well as the degree of co-occurrence of multiple elements (Fig. 2C). Moreover, international trade of food products originating from high-risk countries may lead to a spillover effect and dispersion of such risks (Fig. 1D).

Our study identified a notable high-risk zone in low-latitude Eurasia and across southern Europe, the Middle East, South Asia, and southern China. This belt coincides with the geographical distribution of several ancient cultures, including ancient Greek civilizations, the Roman Empire, Persian culture, ancient India, and Yangtze River Chinese culture (fig. S25). This intercontinental "metal-enriched corridor" is attributed to a combination of anthropogenic and environmental factors (discussed below). Because metals do not degrade, this zone can be regarded as a keystone indicator of the Anthropocene era.

Natural and anthropogenic drivers

Several environmental drivers affect the global distribution of toxic metal exceedances. Near-surface temperature, precipitation, and potential evapotranspiration have the strongest positive effects (*38*), likely contributing to relatively high metal exceedance in southern China, India, the Middle East, Central America, and Central Africa. Such conditions accelerate the weathering processes that release metals from soil parent materials and enhance the enrichment of metals in clay minerals and iron oxides or aluminum oxides (*22*). By contrast, the frequency of ground frosts and wet day frequencies show the strongest negative effects (*38*). This may be due to weak weathering-induced influx and strong leaching-related efflux of metals (*39*), as well as weak plant-pump effects limiting vertical enrichment (*17*). The subtropical monsoon climate zones, which are important for global agriculture, tend to be hot and humid despite the dry season. This climate zone has a metal exceedance rate of 34% (−5%/+4%) for the AT, substantially higher than the global average of 15.7%. By contrast, the metal exceedance rate in the cold and humid hemiboreal climate zone is much lower at 6.0% (−2.4%/+5.5%) (Fig. 3B). We also found that high elevation and steep slope landscapes correspond to more prevalent metal exceedance

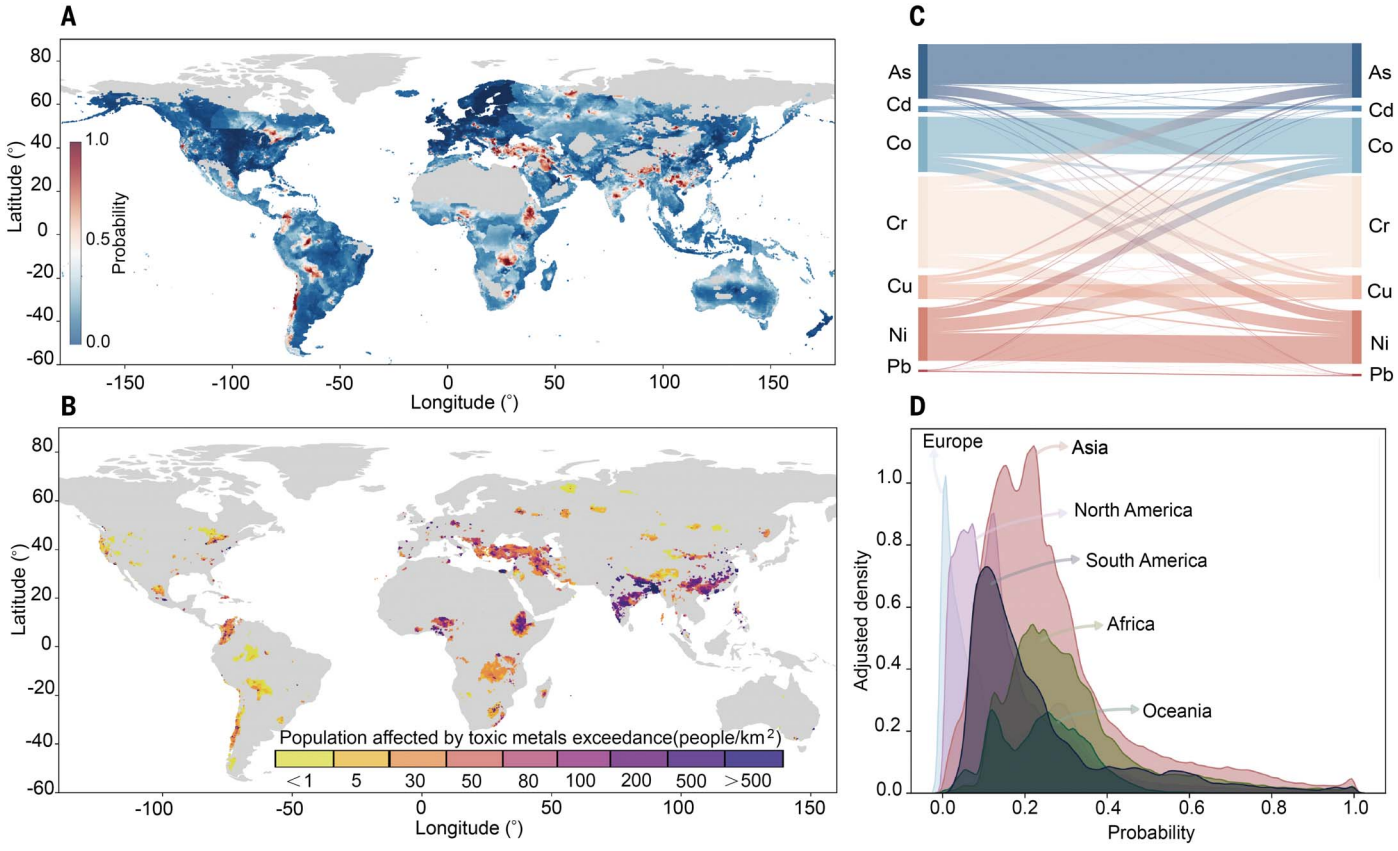

Fig. 2. Global distribution of soil toxic metals exceeding human health and ecological thresholds (HHET). (**A**) Map of metal concentration exceedance. (**B**) Population density in areas with >0.5 probability of metal exceeding ecological and human health threshold. (**C**) Combined soil pollution by toxic metals, with line width in the Sankey diagram showing the proportion of all dual comingled pollution. (**D**) Density histogram showing the relative frequency of exceedance probability of various continents, adjusted by area of each continent.

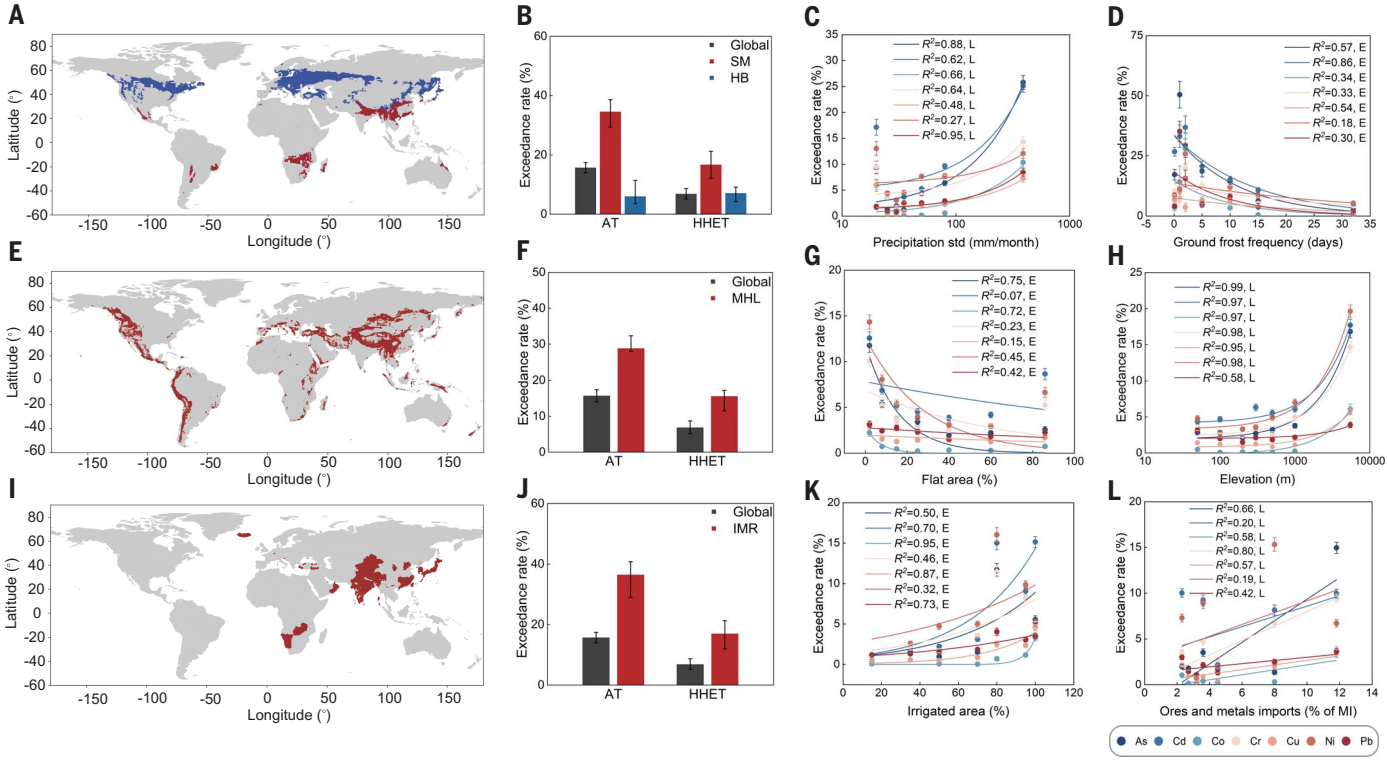

Fig. 3. Natural and anthropogenic drivers of soil metal exceedance. (**A**) Global distribution of subtropical monsoon (SM) (red) and hemiboreal (HB) (blue) climate zones. (**B**) Exceedance rate in global, SM, and HB climate zones. (**C**) Exceedance rate increases as precipitation increases. (**D**) Exceedance rate decreases as ground frost frequency increases. (**E**) Global distribution of hilly mountain areas (HMA), with <2% of area sloped between 0.005 and 0.02, >10% of area sloped between 0.3 and 0.45, and elevation >1000 m above mean sea level. (**F**) Exceedance rate in HMA is significantly higher than the global average. (**G**) Exceedance rate decreases as proportion of flat land increases. (**H**) Exceedance rate increases as elevation increases. (**I**) Global distribution of irrigated and mineral-rich regions (IMR), with proportion of irrigation >90% and ores and metals imports >5% of merchandise imports (MI). (**J**) Exceedance rate in IMR compared with global average. (**K**) Exceedance rate increases as the proportion of irrigation increases. (**L**) Exceedance rate increases as the proportion of ores and metals imports increases. Regression lines are shown in (C), (D), (G), (H), (K), and (L), with "L" indicating linear regression and "E" indicating exponential regression. Error bars represent 95% confidence interval derived from bootstrap method.

(Fig. 3, E to G) owing to the topography affecting rock weathering, soil formation, and erosion, and therefore influencing the leaching and accumulation of metals (*40*–*42*). In mountainous areas with a low percentage of flat areas and high percentage of steep slopes, the metal exceedance rat e is 15% (−4%/+2%) for HHET and 29% (−1%/+3%) for AT, nearly twice the global averages.

Socioeconomic factors are also important drivers governing global toxic metal distribution patterns. Proxies of mining intensity, as identified by ores and metals exports, mineral rents, mineral depletion, and ores and metals imports, were the strongest socioeconomic predictors of toxic metal exceedances, highlighting the major contribution of mining and smelting to metal accumulation in soils at a global scale (*6*, *43*, *44*). The proportion of irrigated land was also found to be a strong predictor of metal exceedance, which is consistent with previous reports that irrigation water contaminated by industrial activities can cause widespread contamination of agricultural soils (*6*, *8*, *19*). In areas with intensive mining activities and a high percentage of surface irrigation (Fig. 3, I to L), the metal exceedance rate was 17% (−5%/+4%) for HHET and 36% (−7%/+4%) for AT, more than twice the global average. Although irrigation with groundwater extracted from arsenic-bearing aquifers in the region south of the Himalayas resulted in hot spots of As in soils (*8*), in general, the use of groundwater for irrigation is a strong predictor of toxic metal nonexceedance on a global scale. This suggests that groundwater may generally contain lower levels of toxic metals than other irrigation water sources, thus serving as a carrier of metal efflux rather than influx, except in areas with high geogenic background or serious anthropogenic pollution (*45*).

We used structural equation modeling (SEM) to assess the causal links between irrigation, mining, plant pumping, weathering, leaching, and exceedance rate and hazard level (Fig. 4, A and B, and fig. S22) and found that weathering and plant pumping contribute substantially to the concentrations of As, Cd, Co, and Cu in soil. Furthermore, SEM results verified that anthropogenic processes, including mining and irrigation, provided substantial contributions for most of the toxic metals. Although many effects are exerted through direct influencing pathways, a considerable portion of the influences may be exerted indirectly (Fig. 4C). Indirect pathways account for 96, 87, 62, and 62% of the net effect of mining on hazard level for As, Cd, Co, and Cu. These SEM results were in good accordance with the complex importance features of the machine learning models (Fig. 4D) and support our hypothesis that soil toxic metal enrichment is governed by the interplay of a wide range of biogeophysical and socioeconomic variables at broad spatiotemporal scales.

Discussion

Our model results show that soil contamination is occurring on a global scale, posing major risks to both ecosystems and human health (*7*, *46*) and threatening water quality and food

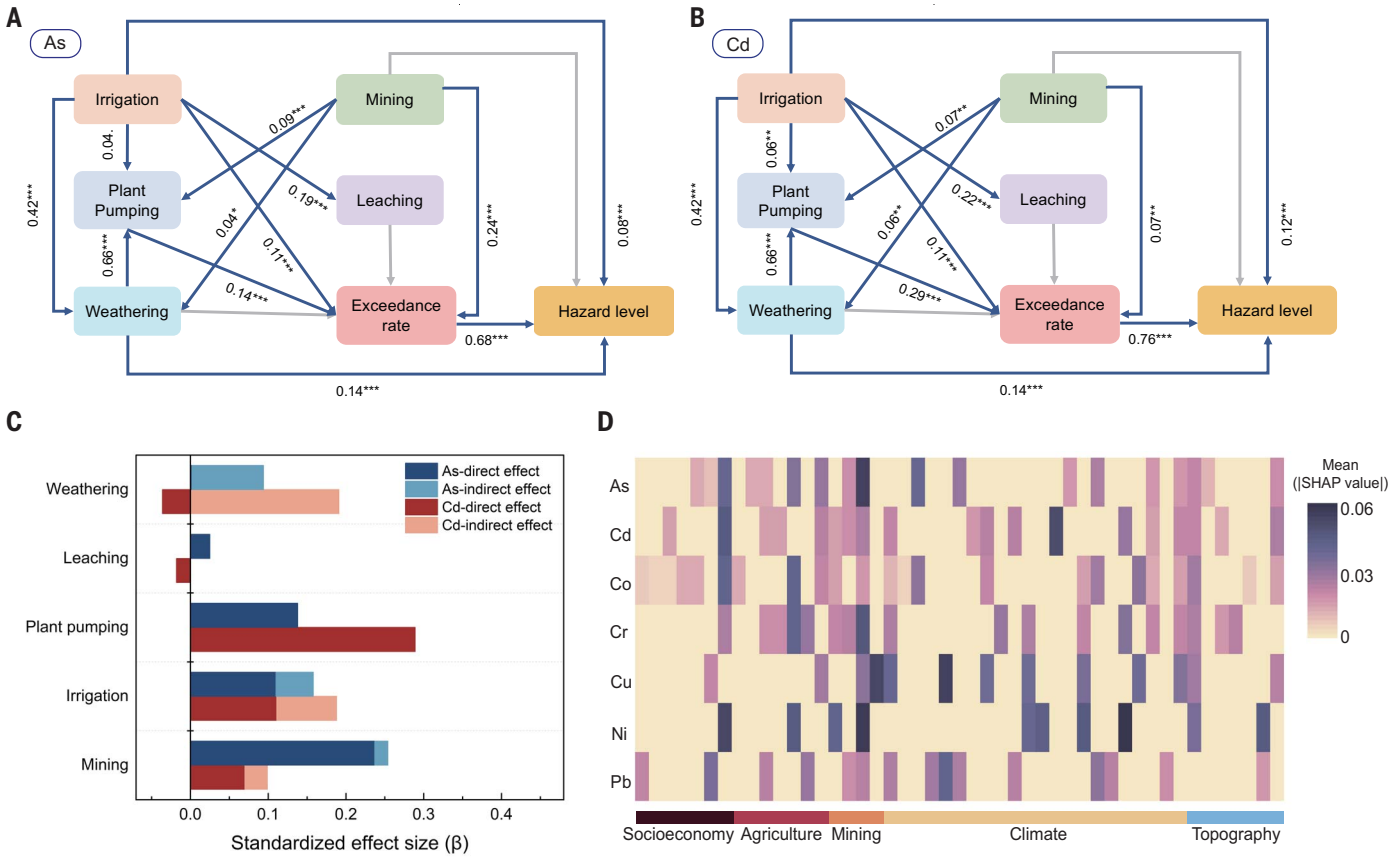

Fig. 4. Relationships among soil metal exceedance and underlying processes. (**A**) Structural equation modeling (SEM) of irrigation, mining, plant pumping effect, leaching, and weathering on exceedance rate and hazard level of As [n = 2149, χ^2 = 4.45, bootstrap P = 0.41, root mean square error of approximation (RMSEA) = 0.04, standardized root mean squared residual (SRMR) = 0.009, goodness-of-fit index (GFI) = 0.999]. $^{**}P < 0.001$, $^{***}P < 0.01$, $^{*}P < 0.05$, $^{\cdot}P < 0.1$. (**B**) SEM of Cd [n = 2379, χ^2 = 0.57, bootstrap P = 0.95, RMSEA = 0.00, SRMR = 0.003, GFI = 1.000]. (**C**) Summed direct effect and indirect effects. The direct effect reflects the degree of standard deviation change in dependent variables with each one standard deviation change in a directly linked predictive variable, and indirect effect reflects the magnitude of associated change through an indirect link. (**D**) Feature importance assessed by Shapley additive explanations (SHAP) (materials and methods 1.4.4). The larger the Shapley value, the more important a variable on the x axis is (*38*).

security (*6*, *8*). The model prediction includes both known soil pollution areas and previously undocumented areas of concern (figs. S23 and S24). Some of these regions, such as Southern China and the Middle East, have been reported previously, but we were able to delineate the risk zones continuously on a global scale. Our machine learning models used data from the public domain to provide an assessment of regional soil pollution, and the results show that the technique is a useful screening tool that can complement traditional soil pollution–mapping methods. There is an ongoing global initiative on soil pollution prevention and restoration under the United Nations Environment Programme (UNEP) and the FAO (*35*, *47*). Our results suggest that international aid should be allocated to facilitate soil pollution surveys in data-sparse regions such as sub-Saharan Africa.

Recent large-scale studies in Europe found a mysterious trend north of the 55° latitude line, which demarcates high-metal soils in the south from the low-metal soils in the north (*11*, *48*). This phenomenon had been attributed to the coincidental match with the maximum extent of the last glaciation; however, the overall mechanism and drivers remain unclear. Our results now reveal that the toxic metal–enriched area across southern Europe is part of a more extensive transcontinental metal-enriched corridor spanning across low-latitude Eurasia (Fig. 1A). We postulate that this corridor of long-lasting legacy of human influence was formed as the result of strong weathering of metal-enriched parent rocks (*12*, *49*) and plant-pumping effects (*13*, *17*), a lower degree of leaching associated with precipitation and terrain (*12*), and a long history of mining and smelting activities occurring since ancient civilizations began (*8*).

Our models were validated by using a series of uncertainty analyses (*26*) (figs. S18 to S21). Mapping the extent of spatial extrapolation showed that our dataset provides a good coverage of most environmental conditions, with the least-represented pixels and highest proportion of extrapolation in Southeast Asia, Russia, and Africa. Due to lack of sampling data in developing countries and remote regions, our model still has relatively high degrees of uncertainty in northern Russia, central India, and Africa (fig. S2). Moreover, metal concentrations in soil have high spatial heterogeneity and may vary considerably over short distances. The present study is based on average metal concentrations on a 10-km grid, which is more reflective of diffusive and regional pollution rather than site-specific conditions. The data may be sufficient for risk screening purposes but are inadequate to support risk mitigation. Soil remediation needs to rely upon site-specific delineation of lateral and vertical extent of soil pollution, as well as a better understanding of metal sources, fate and transport dynamics, and bioavailability (*12*).

Soil pollution can have a profound impact on global food security and public health. For the millions of people making a living on the

14 to 17% of globally polluted cropland, the bioaccumulation of toxic metals in crops and farm animals can affect biodiversity and productivity, cause detrimental health effects, and exacerbate poverty. The collateral effects on the global food chain are unknown at this time, especially in the context of how global trade dynamics may affect the distribution of contaminated agricultural products. These large areas of toxic metal enrichment are expected to continue to increase owing to the growth in demand for critical metals required to support the net zero "green transition" and the development of photovoltaic devices, wind turbines, and electric vehicle batteries (*50*, *51*). We hope that the global soil pollution data presented in this report will serve as a scientific alert for policy-makers and farmers to take immediate and necessary measures to better protect the world's precious soil resources.

REFERENCES AND NOTES

1. Food and Agriculture Organization of the United Nations, "Healthy soils are the basis for healthy food production" (FAO, 2015).
2. M. van Dijk, T. Morley, M. L. Rau, Y. Saghai, *Nat. Food* **2**, 494–501 (2021).
3. United Nations Convention to Combat Desertification, *Global Land Outlook* (UNCCD, 2017).
4. Food and Agriculture Organization of the United Nations, *Status of the World's Soil Resources* (FAO, 2015).
5. Food and Agriculture Organization of the United Nations, "Saving our soils by all earthly ways possible" (FAO, 2022).
6. D. Hou *et al*., *Nat. Rev. Earth Environ.* **1**, 366–381 (2020).
7. O. Coban, G. B. De Deyn, M. van der Ploeg, *Science* **375**, abe0725 (2022).
8. Food and Agriculture Organization of the United Nations and United Nations Environment Programme, *Global Assessment of Soil Pollution* (FAO and UNEP, 2021).
9. A. Kabata-Pendias, *Trace Elements in Soils and Plants* (CRC Press, 2000).
10. Ministry of Environmental Protection of the People's Republic of China, "National soil contamination survey report" (MEP, 2014).
11. G. Tóth, T. Hermann, G. Szatmári, L. Pásztor, *Sci. Total Environ.* **565**, 1054–1062 (2016).
12. B. J. Alloway, Ed., *Heavy Metals in Soils: Trace Metals and Metalloids in Soils and their Bioavailability* (Springer Dordrecht, ed. 3, 2013).
13. A. A. Meharg, C. Meharg, *Environ. Sci. Technol.* **55**, 7757–7769 (2021).
14. J. Podgorski, M. Berg, *Science* **368**, 845–850 (2020).
15. J. O. Nriagu, *Nature* **338**, 47–49 (1989).
16. X. Liu *et al*., *Nat. Rev. Earth Environ.* **3**, 461–476 (2022).
17. M. Imseng *et al*., *Environ. Sci. Technol.* **52**, 1919–1928 (2018).
18. S. Hong, J.-P. Candelone, C. C. Patterson, C. F. Boutron, *Science* **272**, 246–249 (1996).
19. M. G. Macklin *et al*., *Science* **381**, 1345–1350 (2023).
20. S. Hong, J.-P. Candelone, C. C. Patterson, C. F. Boutron, *Science* **265**, 1841–1843 (1994).
21. J. O. Nriagu, J. M. Pacyna, *Nature* **333**, 134–139 (1988).
22. M. Imseng *et al*., *Environ. Sci. Technol.* **53**, 4140–4149 (2019).
23. L. R. Lado, T. Hengl, H. I. Reuter, *Geoderma* **148**, 189–199 (2008).
24. S. Maas *et al*., *Environ. Pollut.* **158**, 2294–2301 (2010).
25. Y. Hu, H. Cheng, *Environ. Sci. Technol.* **47**, 3752–3760 (2013).
26. Materials and methods are available as supplementary materials.
27. P. Geurts, D. Ernst, L. Wehenkel, *Mach. Learn.* **63**, 3–42 (2006).
28. British Geological Survey, *World Mineral Production 2016–2020* (BGS, 2022).
29. A. Kubier, R. T. Wilkin, T. Pichler, *Appl. Geochem.* **108**, 1–16 (2019).
30. BGS, "Mineral profile: Nickel" (British Geological Survey, 2008).
31. G. Gunn, Ed., *Critical Metals Handbook* (John Wiley & Sons, 2013).
32. H. Chen, Y. Teng, S. Lu, Y. Wang, J. Wang, *Sci. Total Environ.* **512-513**, 143–153 (2015).
33. N. Gupta *et al*., *Environ. Toxicol. Pharmacol.* **82**, 103563 (2021).
34. M. Amini, M. Afyuni, N. Fathianpour, H. Khademi, H. Flühler, *Geoderma* **124**, 223–233 (2005).
35. United Nations Environment Assembly, "Managing soil pollution to achieve sustainable development," UNEA3/6 (Third Session, Resolution 6) (UNEA, 2018).
36. G. Liu *et al*., *Geoderma* **312**, 104–113 (2018).
37. G. Lin *et al*., *J. Hazard. Mater.* **480**, 135876 (2024).
38. D. Hou *et al*., Global soil pollution by toxic metals threatens agriculture and human health, Dryad (2025); https://doi.org/10.5061/dryad.83bk3jb2z.
39. F. Meite *et al*., *Sci. Total Environ.* **616–617**, 500–509 (2018).
40. W. E. Dietrich, J. T. Perron, *Nature* **439**, 411–418 (2006).
41. C. Boente *et al*., *Catena* **208**, 105730 (2022).
42. Q. Ding, G. Cheng, Y. Wang, D. Zhuang, *Sci. Total Environ.* **578**, 577–585 (2017).
43. A. S. Vega *et al*., *Appl. Geochem.* **141**, 105230 (2022).
44. E. Saljnikov *et al*., *Environ. Geochem. Health* **41**, 2265–2279 (2019).
45. T. Gleeson, M. Cuthbert, G. Ferguson, D. Perrone, *Annu. Rev. Earth Planet. Sci.* **48**, 431–463 (2020).
46. United Nations Environment Programme, *Towards a Pollution-Free Planet: Background Report* (UNEP, 2017).
47. Food and Agriculture Organization of the United Nations, *Soil Pollution: A Hidden Reality* (FAO, 2018).
48. C. Reimann, P. de Caritat, GEMAS Project Team, NGSA Project Team, *Sci. Total Environ.* **416**, 239–252 (2012).
49. H. S. Moghadam *et al*., *J. Petrol.* **58**, 2143–2190 (2017).
50. K. Bhuwalka *et al*., *Environ. Sci. Technol.* **55**, 10097–10107 (2021).
51. A. Farina, A. Anctil, *Resour. Conserv. Recycling* **176**, 105938 (2022).

ACKNOWLEDGMENTS

We thank the anonymous reviewers for their constructive comments and the many providers of data used in our models. **Funding:** This work was supported by National Natural Science Foundation of China grant 42225703 (D.H.) and National Key Research and Development Program of China grant 2020YFC1808000 (D.H.).
Author contributions: Conceptualization: D.H., X.J., S.P.M., Y.-G.Z, Q.H., F.-J.Z., M.S.B., D.O., J.N.; Funding acquisition: D.H.; Investigation: D.H., X.J., L.W.; Methodology: D.H., X.J., L.W., S.P.M., F-J.Z., D.O.; Project administration: D.H., L.W.; Visualization: D.H., X.J.; Supervision: D.H.; Writing – original draft: D.H., X.J.; Writing – review & editing: D.H., S.P.M., Y.-G.Z., Q.H., F.-J.Z., M.S.B., D.O., J.N. **Competing interests:** The authors declare that they have no competing interests. **Data and materials availability:** Data and code generated during this study are publicly available and can be accessed at (*38*).

SUPPLEMENTARY MATERIALS

science.org/doi/10.1126/science.adr5214
Materials and Methods
Figs. S1 to S27
Tables S1 to S10
References (*52–128*)
MDAR Reproducibility Checklist

Submitted 4 July 2024; resubmitted 19 November 2024
Accepted 5 March 2025
10.1126/science.adr5214